Journal of Porphyrins and Phthalocyanines
J. Porphyrins Phthalocyanines 2019; **23**: 1–8
DOI: 10.1142/S1088424619501104

Published at http://www.worldscinet.com/jpp/

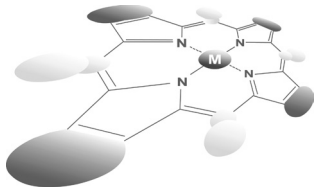

meso-(2-Benzimidazolyl)-substituted BODIPYs: Synthesis, structures and spectroscopic properties

Hu Gao, Chenhong Li and Zhen Shen*

State Key Laboratory of Coordination Chemistry, School of Chemistry and Chemical Engineering, Nanjing University, Nanjing 210046, China

Dedicated to Professor Atsuhiro Osuka on the occasion of his 65th birthday.

Received 25 May 2019
Accepted 2 August 2019

ABSTRACT: A series of *meso*-(2-benzimidazolyl)-substituted boron dipyrromethene (BODIPY) derivatives **3a–3c** and **4** have been synthesized and characterized. The absorption and fluorescence bands of **3a** are bathochromically shifted by 36 nm and 61 nm, respectively, compared with those of the *meso*-phenyl BODIPY in toluene. More importantly, the fluorescence quantum yields of these *meso*-(2-benzimidazolyl)-substituted BODIPYs (up to 0.45 in toluene) are much higher than those of the previously reported *meso*-heterocyclic BODIPYs. X-ray crystallographic analysis of the single crystal structure of **3a** revealed that the dihedral angle of *meso*-benzimidazolyl ring and indacene plane (40.47°) is smaller compared with that of the *meso*-tolyl substituted BODIPY (61.4°). Replacement of the six-membered ring with a five-membered ring, as well as the absence of hydrogen at the imino-nitrogen, generated the reduced repulsion and the hydrogen bonding interaction. The increased planarity not only provided the substantial delocalization of π electrons and red shifted the absorption and emission bands but also enhanced the fluorescence quantum yield by reducing free rotation induced nonradiative deactivation pathway. Furthermore, 3,5-distyryl coupled BODIPY **4** exhibits a NIR fluorescence band at 712 nm with moderate quantum yield ($\Phi_F > 0.3$) in nonpolar and polar solvents, which indicate that *meso*-(2-benzimidazolyl) BODIPY acts as a good candidate for post modification toward NIR dyes for biological applications.

KEYWORDS: BODIPY, *meso*-(2-benzimidazolyl), near IR, intramolecular hydrogen bonds.

INTRODUCTION

The development of low-cost NIR region excitation sources and detectors have inspired the design of new fluorophores or fluorescent materials with high molar absorption coefficients and fluorescence quantum yields in the 650–1000 nm region. Boron-dipyrromethene (BODIPY) dyes have received intensive studies over the past two decades owing to their wide range of potential applications in numerous research fields [1, 2]. This has been related to their facile synthesis and structural versatility, excellent spectroscopic properties such as narrow Gaussian-shaped absorption and emission bands, high molar extinction coefficients and fluorescent quantum yields, moderate redox potentials, negligible sensitivity to solvent polarity, excellent photostability, and high solubility in commonly used organic solvents with different polarities [3–7]. The conventional *meso*-aryl substituted BODIPYs absorbed and emitted in the 470–530 nm region [8]. Three main approaches have been identified to shift the main absorption and emission bands to long wavelengths [5, 8]: (i) introduction of aryl, vinyl, styryl and arylethynyl substituents at peripheral positions, (ii) aromatic ring fusion of the pyrrole moiety, and (iii) substitution of a carbon atom with a nitrogen atom at the *meso*-position. Recently, it has been reported that introduction of five membered heterocycles such as pyrrolyl, furyl, thienyl and thiazolyl [9–13] rings instead of six membered aryl groups at *meso*-position of a BODIPY can also affect the optical properties to a

*Correspondence to: Zhen Shen, email: zshen@nju.edu.cn.

great extent. This is mainly because the *meso*-phenyl ring situated almost orthogonally with the indacene plane and made minor contributions to the conjugation of the whole molecule. Replacement of the six-membered ring with a five-membered ring as well as the absence of methyl substituents at the 1,7-positions of a BODIPY can reduce the dihedral angle of the *meso*-substituent and indacene plane due to the reduced repulsion, thus participating in the conjugation [10]. Although these *meso*-heterocyclic BODIPYs exhibited red-shifted absorption and emission bands, they were accompanied by a sharply decreased fluorescence quantum yield (Φ_F < 0.1 in toluene) on account of the electron-donation effect and the twisting motion of the *meso*-heterocyclic rings. This shortcoming restricts their application for post modification to NIR fluorophores. It is well known that imidazole has wide applications in optical materials and biological fields because of its π-conjugated cyclic system and bioactivity [14]. Herein we describe the synthesis, structures and spectroscopic properties of *meso*-(2-benzimidazolyl) BODIPY derivatives **3a–3c**. Meanwhile, we also investigated its distyryl coupled dye **4** which emits strongly in the NIR region with moderate fluorescence quantum yield.

RESULTS AND DISCUSSION

Synthesis and characterization

The synthetic procedures for BODIPYs **3a–3c**, **4** and the dipyrromethane precursors **2a–2c** are described in Scheme 1. The starting materials, 2-hydroxymethyl-benzimidazole **1a–1c**, were prepared according to the literature [15]. Recently, Werz and co-workers reported a method for synthesizing this kind of dipyrromethanes and their BF_2-complexes with the participation of benzimidazole auxochrome [16]. Compounds **1a–1c** were converted to their respective formaldehydes using 2-iodobenzoic acid (IBX) followed by *in situ* condensation with 2-methylpyrrole. A mixed medium consisting of DMSO and *N*-methyl-2-pyrrolidone (NMP) as well as excess amounts of TFA was used to dissolve the carbaldehyde intermediates and neutralize the evolving basicity of products. Compounds **2a–2c** were obtained in 35–50% yields. Finally, the target BODIPYs **3a–3c** were obtained by adding only one-third amount of 1,8-diazabicyclo[5.4.0]undec-7-ene (DBU) and $BF_3 \cdot OEt_2$ according to the literature in 50–58% yields. The Knoevenagel condensation reaction of BODIPY **3a** and 4-*tert*-butylbenzaldehyde affords the distyryl expanded dye **4** in 75% yield [17]. The structures of **3a–3c** and **4** have been characterized by ^1H, ^{13}C NMR and HR-MS spectroscopy.

Crystal structure

The structure of **3a** was confirmed by X-ray crystallographic analysis. An orange-colored single crystal for **3a** was obtained by slow diffusion of *n*-hexane into a dichloromethane solution at room temperature. Compound **3a** was crystallized in the asymmetric monoclinic unit cell with $P2_1/c$ space group and the crystal structure is shown in Fig. 1. The highly planar BODIPY framework is composed of two pyrrole rings at the periphery and a central six-membered ring containing a coordinated boron atom. The dihedral angle between the central indacene core and the *meso*-benzimidazolyl ring is

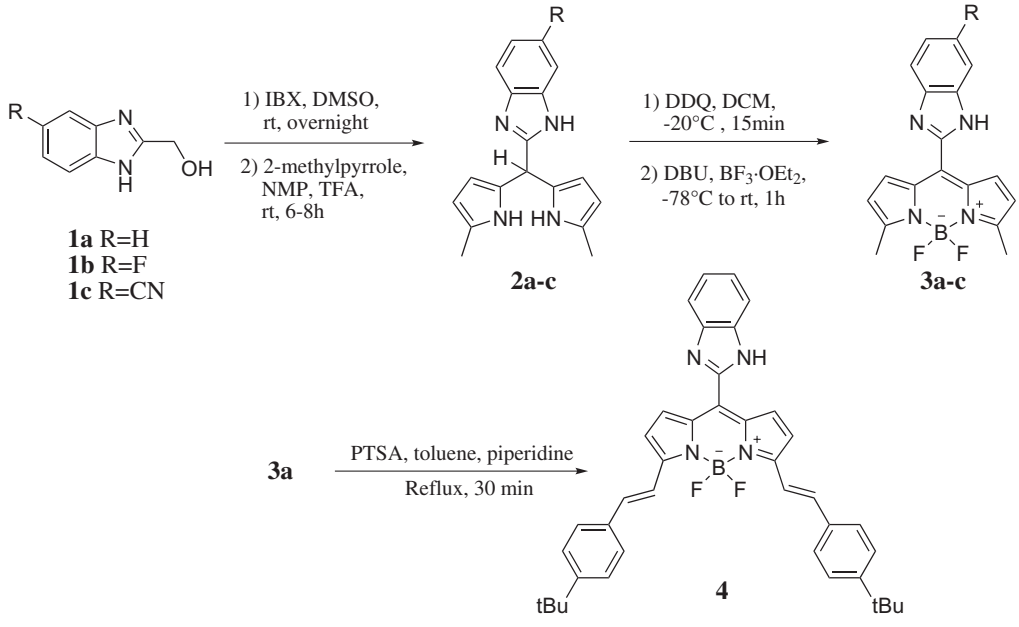

Scheme 1. Synthetic procedures and structures of BODIPYs **3a–3c** and **4**

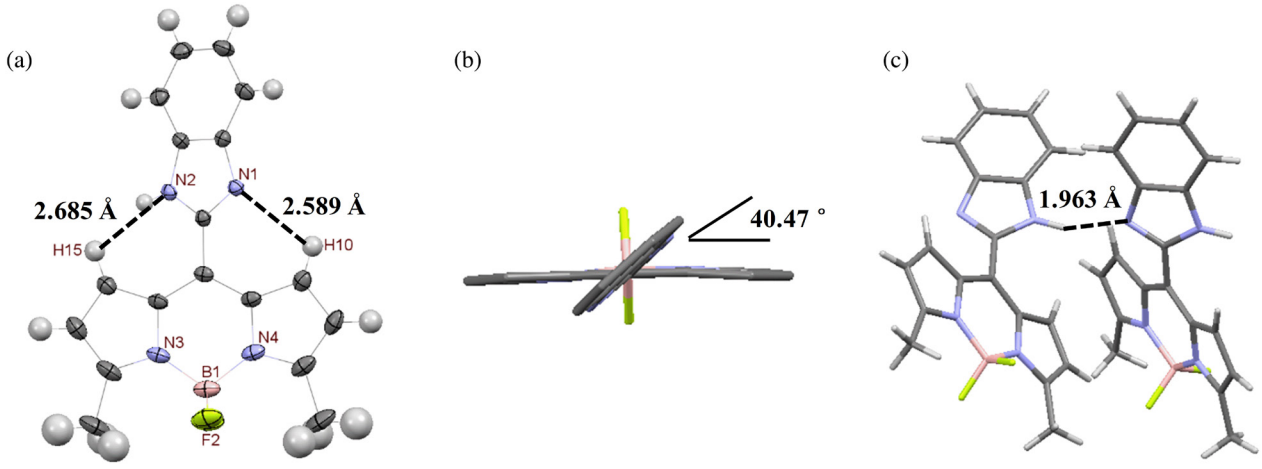

Fig. 1. X-Ray crystal structure of **3a** with the thermal ellipsoids set at 50% probability level. (a) Top view; (b) Side view; (c) dimeric structure formed by intermolecular hydrogen bonding. Solvent molecules are omitted for clarity

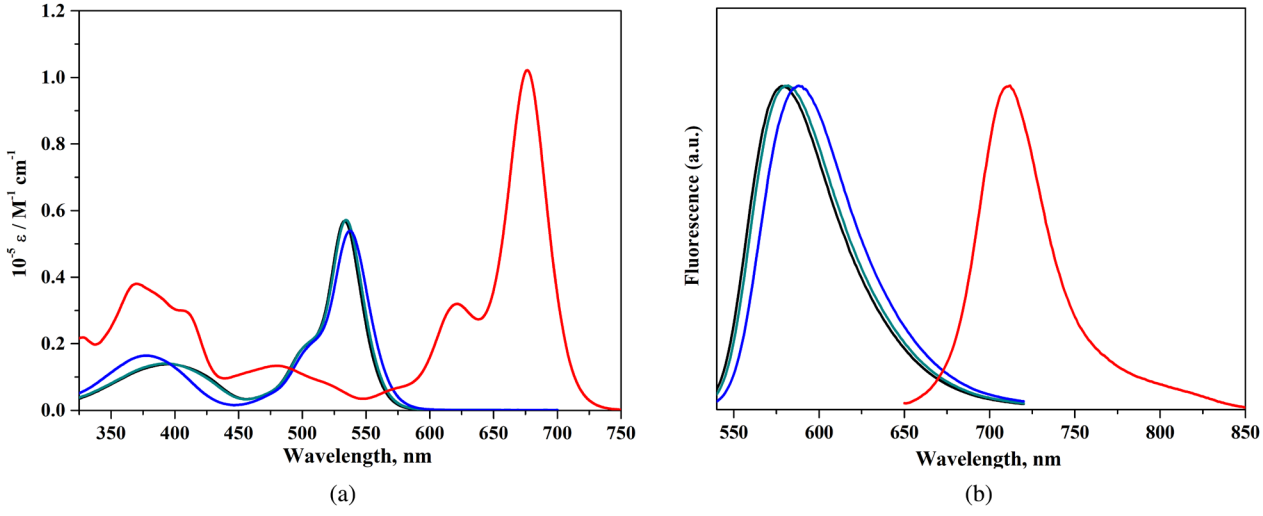

Fig. 2. The UV-vis absorption (a) and normalized emission (b) spectra of dyes **3a** (black), **3b** (green), **3c** (blue) and **4** (red) in toluene ($c = 1 \times 10^{-5}$ M) (λ_{ex} = 515 nm for **3a–3c** and λ_{ex} = 645 nm for **4**)

40.47°, which is smaller than that of *meso*-tolyl BODIPY (61.4°), but larger than that of *meso*-pyrrolyl BODIPY (33.94°) [10]. There are two intramolecular hydrogen bonding interactions between the nitrogen atoms from the benzimidazolyl ring and the proximal proton atoms from the indacene core (N1–H10 = 2.589 Å, N2–H15 = 2.685 Å), which imposes restrictions on the twisting motion of the benzimidazolyl ring and facilitates the molecule to adopt a stable, partly coplanar conformation. The enhanced planarity of the whole π-conjugated structure would promote greater π-electron density delocalization, and thus enhanced optical characteristics [12]. In the solid state, the intermolecular hydrogen bonding interactions N2-H···N1 (1.963 Å) (N2-H of a *meso*-benzimidazolyl moiety and N1 of another *meso*-benzimidazolyl moiety) between the neighboring BODIPY molecules forms a dimeric structure.

Spectroscopic properties in solution

The photophysical properties of compounds **3a–3c** and **4** were measured in five solvents of different polarity and the data were summarized in Fig. S17 and Table S1. The absorption and emission spectra of all the dyes in toluene at the same concentration is shown in Fig. 2 and Table 1. Compounds **3a–3c** display absorption maxima at 533, 534 and 537 nm, respectively, with similar intensity, which can be assigned to a typical S_0–S_1 transition of BODIPY [18]. Other higher-energy absorption bands around 300–450 nm are shown broadly, which can be attributed to S_0–S_2 or S_0–S_3 transition. Compound **4** exhibits a narrow and strong absorption band at 676 nm with an obvious shoulder at 621 nm, which is red shifted by 143 nm relative to that of **3a**. Meanwhile, the absorbance of **4** is significantly increased as the molar absorption coefficient

Table 1. Spectroscopic and photophysical properties of dyes **3a–3c** and **4** in toluene at 298k

	Solvents	λ_{abs} [nm]	λ_{em} [nm]	$\varepsilon_{max} \times 10^4$ [$M^{-1} \cdot cm^{-1}$]	$\Delta\nu$ [cm^{-1}]	Φ_F	τ_f [ns]
3a	Toluene	533	578	5.65	1461	0.45	4.83
3b	Toluene	534	582	5.7	1544	0.41	4.47
3c	Toluene	537	588	5.4	1615	0.36	4.05
4	Toluene	676	712	10.3	748	0.31	3.72

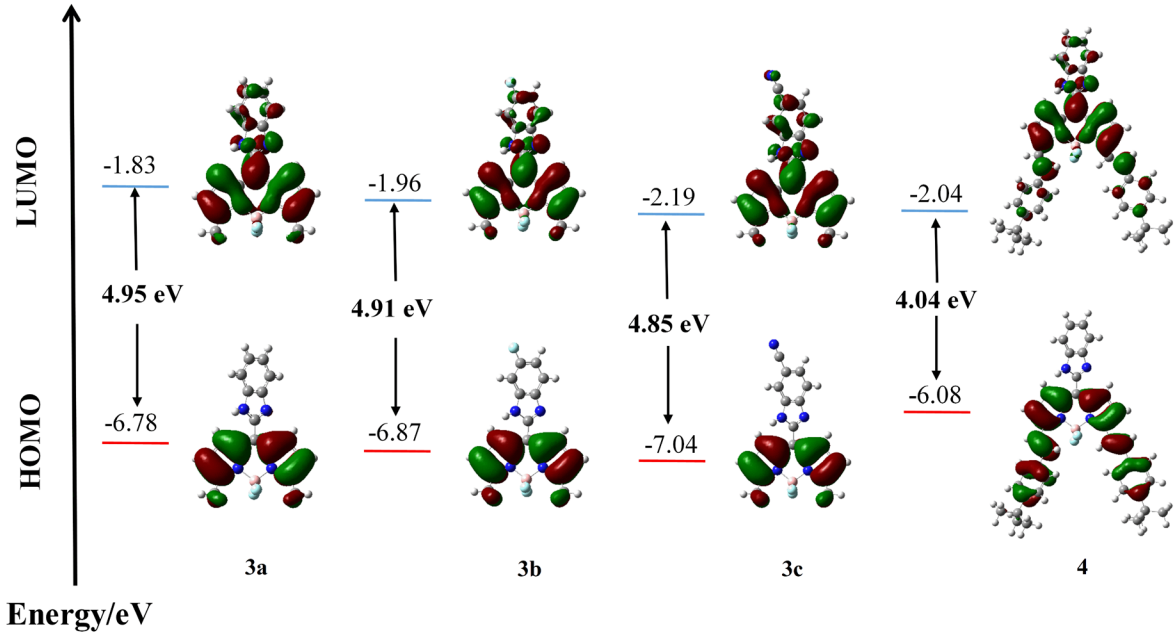

Fig. 3. Energy level diagrams and Kohn–Sham orbital representation of LUMOs (top) and HOMOs (bottom) of **3a–3c** and **4** using the CAM-B3LYP functional and 6-31G (*d*, *p*) basis set

at 676 nm ($\varepsilon = 1.03 \times 10^5 M^{-1} \cdot cm^{-1}$) is 1.82-fold compared to that of **3a** at 578 nm ($\varepsilon = 5.65 \times 10^4 M^{-1} \cdot cm^{-1}$). This is due to the increased π conjugation by coupling two styryl-groups at 3,5-positions. In addition, the absorption maximum of **3a–3c** and **4** is slightly dependent on the polarity of the solvent, with slight blue shifts with the increase of solvent polarity, which is in line with the properties of BODIPY systems.

The emission spectra were obtained by excitation at optimal wavelength, which exhibit approximate mirror symmetry with the main absorption bands. In toluene, compounds **3a–3c** show a maximum fluorescence peak at 578, 582 and 588 nm, respectively, with decent quantum yields (Φ_F) of 0.45, 0.41 and 0.36, respectively. The introduction of electron withdrawing groups (-F and -CN) on the benzimidazolyl moiety results in a further red shift in absorption and emission spectra, with a larger Stokes shift and reduced Φ_F value. Compared with the *meso*-phenyl BODIPY, the emission band of **3a** is red shifted by 61 nm and the Stokes shift is increased by 683 cm^{-1} [19], which fully illustrates that the replacement of the six-membered aryl group with the five-membered aromatic heterocycle at the *meso*-position significantly alters the optical characteristics of BODIPYs. In addition, the Φ_F values of compounds **3a–3c** are much higher than those of the previously reported *meso*-heterocyclic BODIPYs. It is likely that the intramolecular hydrogen bonds limit the free rotation of the benzimidazolyl ring, thereby decreasing the incidence of nonradiative decay. The distyryl coupled compound **4** displays a maximum fluorescence peak at 712 nm in the NIR region and maintains Φ_F value over 0.3 in all investigated solvents, which suggests that *meso*-(2-benzimidazolyl) BODIPY can be post-modified to novel NIR BODIPY dyes. Furthermore, the fluorescence decay profiles of **3a–3c** and **4** can be described by mono-exponential fits with lifetimes. The radiative (k_r) and nonradiative (k_{nr}) rate constants are calculated using Φ_F and fluorescence lifetime values.

It is well known that benzimidazole is sensitive to pH changes and can be protonated in acidic environments [20]. The pH-dependent absorption and emission spectra were studied by titration of trifluoroacetic acid (TFA) into the CH_2Cl_2 solution of **3a** (Fig. S18). Upon addition

Table 2. Calculated electronic excitation energies, oscillator strengths, and eigenvectors for the TD-DFT spectra of **3a–3c** and **4** carried out using the CAM-B3LYP functional and 6-31G (*d*, *p*) basis set

	State[a]	E[b] (eV)	λ (nm)	f[c]	Orbitals(coefficient)[d]
3a	S1	2.96	420	0.457	H→L (97%), H-3→L (2%)
	S2	3.69	336	0.354	H-1→L (89%), H-3→L (6%)
3b	S1	2.89	429	0.444	H→L (97%)
	S2	3.62	343	0.413	H-1→L (93%)
3c	S1	2.86	434	0.441	H→L (97%)
	S3	3.86	322	0.357	H-1→L (55%), H-3→L (40%)
4	S1	2.24	554	0.721	H→L (97%)
	S2	3.26	381	1.217	H-1→L (90%), H-2→L (4%)

[a]Excited states. [b]Energy of excited states. [c]Oscillator strength (f < 0.02 are not included). [d]MOs involved in the transitions with H and L denoting the HOMO and LUMO, respectively.

of TFA, the absorption intensity at 533 nm decreased with a new band at 548 nm appearing concomitantly. The fluorescence quantum yield of **3a** decreased almost 4-fold (22%) in the presence of 0.2 equiv. of TFA, and dropped to 6% upon addition of 1 equiv. of TFA. This indicates that the protonated benzimidazole moiety quenches the fluorescence of the BODIPY significantly. This phenomenon can be explained by theoretic calculations (Fig. S19). In the neutral form, the HOMO energy level of the benzimidazole subunit (-5.89 eV) is slightly lower than that of the indacene moiety (-5.53 eV), while its LUMO energy level (-0.22 eV) is much higher than that of the indacene moiety (-2.51 eV). Therefore, no photo-induced electron transfer (PET) will take place between the benzimidazole and indacene core. However, after protonation, the LUMO energy level (-5.42 eV) of the protonated benzimidazole becomes much lower than that of the indacene moiety. Thus, upon photoexcitation of the indacene core, the intramolecular electron transfer from the LUMO of the indacene moiety to the LUMO of the protonated benzimidazole becomes energetically favorable. The fluorescence of **3a** in the protonated form is quenched through an oxidative PET process.

DFT calculations

To derive an enhanced understanding of the electronic and spectroscopic properties of **3a–3c** and **4**, density functional theory (DFT) calculations at the CAM-B3LYP/6-31G (*d*, *p*) level were carried out. The plots and data for the HOMOs and LUMOs are shown in Fig. 3 and Table 2. The general trends of the calculated HOMO/LUMO levels and energy gaps are in line with the experimentally observed trends in solution. In the HOMO depictions, there is a nodal plane at the *meso*-carbon in all *meso*-(2-benzimidazolyl) BODIPYs, indicate that the *meso*-benzimidazole ring has only a minor effect on the energy of the HOMO. However, the *meso*-substituent has a significant impact on the energy of the LUMO, since there is a large MO coefficient at this position. The calculations for compounds **3a–3c** display that the delocalized HOMO distributes only over the indacene core, while delocalized LUMO distributes over the indacene core and partial *meso*-benzimidazolyl moiety. As the electron withdrawing ability of the substituent on the benzimidazolyl ring increases, both the HOMO and LUMO energy levels are further stabilized with a slightly decreased HOMO–LUMO gap. This is consistent with the slight red shift of the absorption and emission spectra of **3b** and **3c**. Compared with **3a**, the remarkable narrowing of the HOMO–LUMO gap of compound **4** is mainly owing to the destabilization of the HOMO *via* coupling with distylyl substituents, leading to an apparent red shift of the absorption and emission bands.

CONCLUSION

In summary, we have synthesized and characterized a series of *meso*-(2-benzimidazolyl) BODIPY derivatives **3a–3c** and **4**. The absorption and fluorescence bands of **3a** are centered at 533 nm and 578 nm, which are bathochromically shifted by 36 nm and 61 nm, respectively, compared with the *meso*-phenyl BODIPY in toluene. Surprisingly, its fluorescence quantum yield is up to 0.45 in toluene, which is much higher than those of previously reported *meso*-heterocyclic BODIPYs. It is likely that the intramolecular hydrogen bonds limit the rotation of the benzimidazolyl ring, thereby decreasing the incidence of nonradiative decay. In addition, the distyryl-coupled BODIPY **4** absorbs at 676 nm and shows a fluorescence band at 712 nm in toluene along with Φ_F value over 0.3 in both nonpolar and polar solvents,

which suggests that *meso*-(2-benzimidazolyl) BODIPY can be used as a good platform for post modification to achieve NIR dyes for various applications in material and biological sciences.

EXPERIMENTAL

Instrumentation and materials

All chemical reagents were obtained from commercial suppliers and used directly, unless otherwise mentioned. The NMR spectra of all compounds were measured on a Bruker DRX 500 or 400 spectrometer at 298k and referenced to the residual proton signals of the CD_3Cl or DMSO-d_6. The HR-MS data were recorded (in negative ion mode) on an Agilent 6540 Q-TOF LC/MS spectrometer. All the solvents employed for the spectroscopic measurements were of UV spectroscopic grade (Aldrich).

Synthesis

***Preparation of dipyrromethanes* (2b–2c).** 2-Hydroxymethylbenzimidazole **1b** (2.50 mmol, 1.0 equiv.) was added to a solution of 2-iodoxybenzoic acid (IBX) (2.75 mmol, 1.1 equiv.) in 5 mL dimethyl sulfoxide (DMSO). The mixture was stirred at room temperature under N_2 atmosphere overnight. Next the reaction mixture was diluted with 10.0 mL *N*-methyl-2-pyrrolidone (NMP). Trifluoroacetic acid (TFA) (1.50 mmol, 0.6 equiv.) was added and subsequently the 2-methylpyrrole (7.50 mmol, 3.0 equiv.) as liquid diluted with little NMP. Stirring continued for 8 h at room temperature under a N_2 atmosphere. Afterwards, the reaction mixture was washed with saturated $NaHCO_3$ solution first, then with saturated NaCl solution to remove the remainders of DMSO and NMP with high boiling points and extracted with ethyl acetate. The organic layer was dried over Na_2SO_4 and evaporated to dryness under vacuum. Finally, the crude product was purified by column chromatography (silica gel, dichloromethane/0.5% methanol) and recrystallized from dichloromethane/*n*-hexane to give **2b** as pink powders. Yield 380 mg (50%). ^{1}H NMR (400 MHz, $CDCl_3$) δ: 8.74 (s, 2H), 7.39 (dd, J = 8.8, 4.7 Hz, 1H), 7.15 (dd, J = 8.9, 2.5 Hz, 1H), 6.96 (td, J = 9.2, 2.5 Hz, 1H), 5.94 (t, J = 3.0 Hz, 2H), 5.82–5.81 (m, 2H), 5.62 (s, 1H), 2.21 (s, 6H). HR-MS (ESI-Q-TOF): *m/z* $C_{18}H_{16}FN_4^-$ [M–H]$^-$ calcd. 307.1364, found 307.1366.

Compound **2c** could not be isolated in pure form, apparently, because of its high sensitivity to oxidation. The synthesis follows the general reaction procedure similar to that of **2b** and the reaction time was 6 h. The crude product, obtained in *ca.* 35% yield, was submitted to the next BODIPY synthesis. HR-MS (ESI-Q-TOF): *m/z* $C_{19}H_{16}N_5^-$ [M–H]$^-$ calcd. 314.1411, found 314.1402.

***Preparation of BODIPYs* (3a–3c).** Dipyrromethane **2a** (1.00 mmol, 1.0 equiv.) was dissolved in dry dichloromethane (60.0 mL) under a N_2 atmosphere. The reaction mixture was cooled to -20 °C. A suspension of DDQ (1.1 mmol, 1.1 equiv.) in a mixed solution of 2.00 mL toluene and 2.00 mL dichloromethane was added to the previous mixture. Stirring continued for 15 min at -20 °C. After cooling to -78 °C, 1, 8-diazabicyclo[5.4.0] undec-7-ene (DBU) (10.0 mmol, 10 equiv.) was added dropwise under vigorous stirring. After stirring for 5 min, $BF_3 \cdot OEt_2$ (15.0 mmol, 15 equiv.) was added dropwise and stirring continued for 5 min. Finally, the reaction mixture was allowed to warm to room temperature and stirred for a further 1 h. The reaction mixture was quenched by distilled water. The resulting solution was extracted with dichloromethane. The organic layer was dried over Na_2SO_4 and evaporated to dryness under vacuum. The crude residue was separated by column chromatography (silica gel, petroleum ether/25% ethyl acetate), eluting **3a** as a strongly fluorescent fraction and recrystallized from dichloromethane/*n*-hexane to give **3a** as an orange solid. Yield 168 mg (50%). **3a:** ^{1}H NMR (500 MHz, DMSO-d_6) δ: 7.78–7.69 (m, 2H), 7.36 (dd, J = 5.7, 3.6 Hz, 4H), 6.56 (d, J = 4.2 Hz, 2H), 2.59 (s, 6H). ^{13}C NMR (126 MHz, DMSO-d_6) δ: 158.35, 144.94, 133.03, 131.81, 128.80, 123.58, 120.59, 14.74. HR-MS (ESI-Q-TOF): m/z $C_{18}H_{14}BF_2N_4$-[M–H]$^-$ calcd. 335.1285, found 335.1288.

Compounds **3b** and **3c** were obtained by following a procedure similar to that of **3a** in 53% and 58% yield, respectively. **3b**: ^{1}H NMR (400 MHz, DMSO) δ: 13.38 (b, 1H), 7.91–7.37 (m, 2H), 7.33 (d, J = 4.0 Hz, 2H), 7.30–7.13 (m, 1H), 6.55 (d, J = 4.1 Hz, 2H), 2.59 (s, 6H). ^{13}C NMR (126 MHz, DMSO-d_6) δ: 160.23, 158.48, 158.34, 146.27, 132.98, 131.76, 128.50, 120.63, 112.18, 111.98, 99.53, 14.74. HR-MS (ESI-Q-TOF): *m/z* $C_{18}H_{13}BF_3N_4^-$ [M-H]$^-$ calcd. 353.1185, found 353.1191. **3c**: ^{1}H NMR (500 MHz, DMSO-d_6) δ: 8.32 (s, 1H), 7.87 (d, J = 8.4 Hz, 1H), 7.73 (dd, J = 8.4, 1.5 Hz, 1H), 7.32 (d, J = 4.2 Hz, 2H), 6.57 (d, J = 4.3 Hz, 2H), 2.60 (s, 6H). ^{13}C NMR (126 MHz, DMSO-d_6) δ: 159.07, 148.06, 133.09, 131.76, 127.85, 126.58, 120.88, 119.68, 105.20, 14.79. HR-MS (ESI-Q-TOF): *m/z* $C_{19}H_{13}BF_2N_5^-$ [M–H]$^-$ calcd. 360.1238, found 360.1239.

***Preparation of BODIPY* (4).** A solution of *meso*-(2-benzimidazolyl) BODIPY **3a** (0.15 mmol, 1.0 equiv.) and 4-*tert*-butylbenzaldehyde (0.375 mmol, 2.5 equiv.) in a mixture of 30 mL toluene, *p*-toluenesulfonic acid (PTSA) (3 mg) and pyridine (0.2 mL) were placed in a round-bottom flask equipped with a Dean–Stark trap, and the mixture was heated under reflux until it evaporated to dryness. After cooling for 15 min, the resulting combined solid was dissolved in dichloromethane and washed with water. The organic layer was dried over Na_2SO_4 and evaporated to dryness under vacuum, and the crude residue was separated by column chromatography (silica gel, petroleum ether/10% ethyl acetate) and

recrystallized from tetrahydrofuran/*n*-hexane to give **4** as purple powders. Yield 70 mg (75%). ^{1}H NMR (500 MHz, DMSO-d_6) δ: 7.81–7.72 (m, 4H), 7.65–7.58 (m, 6H), 7.53 (d, J = 8.5 Hz, 4H), 7.48 (d, J = 4.5 Hz, 2H), 7.39 (d, J = 4.5 Hz, 2H), 7.36 (dt, J = 7.2, 3.6 Hz, 2H), 1.32 (s, 18H). ^{13}C NMR (126 MHz, DMSO-d_6) δ: 154.84, 152.73, 145.45, 138.23, 134.94, 133.43, 130.89, 127.28, 126.07, 125.19, 123.48, 117.89, 117.65, 34.68, 30.96. HR-MS (ESI-Q-TOF): *m/z* $C_{40}H_{38}BF_2N_4^-$ [M–H]$^-$ calcd. 623.3163, found 623.3165.

X-ray structure determination

The X-ray diffraction data of **3a** were collected on a Bruker Smart 85 Apex-II CCD diffractometer with graphite monochromated Mo-Kα radiation (l = 0.71073 Å) using the ω-2θ scan mode. The structure was solved by direct methods and refined on F^2 with the full-matrix least-squares method using SHELX programs. All calculations and molecular graphics were carried out using the SHELX-97 program package and the Mercury program.

3a. $C_{18}H_{15}BF_2N_4$, CH_2Cl_2: an orange block-like crystal of the approximate dimensions 0.22 × 0.19 × 0.17 mm^3 was measured. Monoclinic, space group $P2(1)/c$, a = 11.069 (2) Å, b = 17.359 (3) Å, c = 10.1105 (16) Å, α = 90, β = 99.650 (5), γ = 90, V = 1915.2 (6) Å^3, Z = 4, $F(000)$ = 864.0, ρ = 1.460 g·cm^{-3}, $R1$ = 0.0430, wR_2 = 0.1223, GOF = 1.013, residual electron density between 0.254 and -0.379 eÅ^{-3}.

Spectroscopic measurements

UV-vis absorption spectra were measured on a Shimadzu UV-2550 double beam spectrophotometer. Fluorescence spectra were measured on a Hitachi F-4600 fluorescence spectrophotometer with a xenon arc lamp used as the light source. Absolute fluorescence quantum yields and fluorescence lifetimes were measured on a Horiba Fluorolog-UltraFast spectrophotometer. Absorption and emission measurements of the compounds were carried out in 1 cm × 1 cm quartz cuvettes. For all measurements, the temperature was kept constant at (298 ± 2 K). When the fluorescence decays were monoexponential, the rate constants of radiative (k_r) and nonradiative (k_{nr}) deactivation were calculated from the measured fluorescence quantum yield (Φ_f) and fluorescence lifetime (τ) according to equations (1) and (2):

$$k_r = \Phi_f/\tau \quad (1)$$

$$k_{nr} = (1-\Phi_f)/\tau \quad (2)$$

DFT calculations

The G09W software package [21] was used to carry out a DFT geometry optimization using the CAM-B3LYP functional with 6-31G(d, p) basis sets. The same approach was used to calculate the absorption properties based on the time dependent (TD-DFT) method.

Acknowledgments

We gratefully acknowledge the financial support provided by the National Natural Science Foundation of China (No. 21771102). The theoretical calculations were carried out at the Center for High-Performance Computing in Nanjing University.

Supporting information

A full list of characterization data including HRMS, ^{1}H, ^{13}C NMR spectra, absorption, emission spectra, and X-ray structure details of reported compounds (Figs S1–S19 and Table S1) are given in the supplementary material. This material is available free of charge *via* the Internet at http://www.worldscinet.com/jpp/jpp.shtml. Crystallographic data for compound 3a has been deposited at the Cambridge Crystallographic Data Centre (CCDC) under number CCDC-1909769. Copies can be obtained on request, free of charge, *via* www.ccdc.cam.ac.uk/data_request/cif or from the Cambridge Crystallographic Data Centre, 12 Union Road, Cambridge CB2 1EZ, UK (fax: +44 1223-336-033 or email: deposit@ccdc.cam.ac.uk).

REFERENCES

1. Haugland RP. In *The Handbook. A Guide to Fluorescent Probes and Labeling Technologies*, (*10th ed.*) Molecular Probes, Inc.: Eugene, 2005, pp. 935–947.
2. Valevr B (ed). *Molecular Fluorescence. Principles and Applications*. Wiley-VCH: Weinheim, Germany, 2002.
3. Loudet A and Burgess K. *Chem. Rev.* 2007; **107**: 4891–4932.
4. Ulrich G, Ziessel R and Harriman A. *Angew. Chem., Int. Ed.* 2008; **47**: 1184–1201.
5. Lu H, Mack J, Yang Y and Shen Z. *Chem. Soc. Rev.* 2014; **43**: 4778–4823.
6. Kamkaew A, Lim SH, Lee HB, Kiew LV, Chung LY and Burgess K. *Chem. Soc. Rev.* 2013; **42**: 77–88.
7. Zhao J, Wu W, Sun J and Guo S. *Chem. Soc. Rev.* 2013; **42**: 5323–5351.
8. Zhou Z, Zhou J, Gai L, Yuan A and Shen Z. *Chem. Commun.* 2017; **53**: 6621–6624.
9. Jiang T, Zhang P, Yu C, Yin J, Jiao L, Dai E, Wang J, Wei Y, Mu X and Hao E. *Org. Lett.* 2014; **16**: 1952–1955.
10. Umasekhar B, Ganapathi E, Chatterjee T and Ravikanth M. *Dalton Trans.* 2015; **44**: 16516–16527.
11. Sharma R, Lakshmi V, Chatterjee T and Ravikanth M. *New. J. Chem.* 2016; **40**: 5855–5860.
12. Kim K, Jo C, Easwaramoorthi S, Sung J, Kim DH and Churchill DG. *Inorg. Chem.* 2010; **49**: 4881–4894.

13. Neena KK and Thilagar P. *ChemPlusChem* 2016; **81**: 955–963.
14. Thakare SS, Chakraborty G, More AB, Chattopadhyay S, Mula S, Ray AK and Sekar N. *J. Lumin.* 2018; **194**: 622–630.
15. Alasmary FAS, Snelling AM, Zain ME, Alafeefy AM, Awaad AS and Karodia N. *Molecules* 2015; **20**: 15206–15223.
16. Patalag LJ, Jones PG and Werz DB. *Angew. Chem., Int. Ed.* 2016; **55**: 13340–13344.
17. Wang S, Liu H, Mack J, Tian J, Zou B, Lu H, Li Z, Jiang J and Shen Z. *Chem. Commun.* 2015; **51**: 13389–13392.
18. Kollmannsberger M, Rurack K, Resch-Genger U and Daub J. *J. Phys. Chem. A.* 1998; **102**: 10211–10220.
19. Orte A, Debroye E, Ruedas-Rama MJ, Garcia-Fernandez E, Robinson D, Crovetto L, Talavera EM, Alvarez-Pez JM, Leen V, Verbelen B, Dias de Rezende LC, Dehaen W, Hofkens J, Van der Auweraer M and Boens N. *RSC Adv.* 2016; **6**: 102899–102913.
20. Sevinc G, Kucukoz B, Yilmaz H, Sirikci G, Yaglioglu HG, Hayvali M and Elmali A. *Sens. Actuators B* 2014; **193**: 737–744.
21. *Gaussian 09*. Frisch MJ, TGW, Schlegel HB, Scuseria GE, Robb MA, Cheeseman JR, Scalmani G, Barone V, Mennucci B, Petersson GA, Nakatsuji H, Caricato M, Li X, Hratchian HP, Izmaylov AF, Bloino J, Zheng G, Sonnenberg JL, Hada M, Ehara M, Toyota K, Fukuda R, Hasegawa J, Ishida M, Nakajima T, Honda Y, Kitao O, Nakai H, Vreven T, Montgomery JA Jr, Peralta JE, Ogliaro F, Bearpark M, Heyd JJ, Brothers E, Kudin KN, Staroverov VN, Kobayashi R, Normand J, Raghavachari K, Rendell A, Burant JC, lyengar SS, Tomasi J, Cossi M, Rega N, Millam JM, Klene M, Knox JE, Cross JB, Bakken V, Adamo C, Jaramillo J, Gomperts R, Stratmann RE, Yazyev O, Austin AJ, Cammi R, Pomelli C, Ochterski JW, Martin RL, Morokuma K, Zakrzewski VG, Voth GA, Salvador P, Dannenberg JJ, Dapprich S, Daniels AD, Farkas Ö, Foresman JB, Ortiz JV, Cioslowski J and Fox DJ. Gaussian, Inc.: Wallingford CT, 2009.